Tomislav Jarak
Boris Jalušić
Jurica Sorić

https://doi.org/10.21278/TOF.44101
ISSN 1333-1124
eISSN 1849-1391

MIXED MESHLESS LOCAL PETROV-GALERKIN METHODS FOR SOLVING LINEAR FOURTH-ORDER DIFFERENTIAL EQUATIONS

Summary

The paper presents meshless methods based on the mixed Meshless Local Petrov-Galerkin approach used for solving linear fourth-order differential equations. In all the methods presented here, the primary variable and its derivatives up to the third order are approximated separately. Three different mixed meshless methods are derived by different choices of test and trial functions and are verified using available analytical and reference solutions. The numerical performance of the presented algorithms is demonstrated by several representative numerical examples.

Key words: *meshless, mixed Meshless Local Petrov-Galerkin methods, fourth-order differential equations, thin beams, strain gradient elasticity*

1. Introduction

Typical problems described by fourth-order differential equations include the bending and buckling of thin beams, plates or shells, as well as nonlocal elasticity and plasticity material models based on gradient material theories. In the Finite Element Method (FEM), the solution of fourth-order differential equations in general results in complicated formulations [1]. If these equations are solved by the primal FEM approaches based on the symmetrical weak forms of governing equations, where only the displacement field is approximated, the C1 continuous nodal shape functions are required. In FEM, it is fairly complicated to create such functions even for two-dimensional (2D) problems [2]. As for three-dimensional (3D) problems, deriving efficient C1 FEM formulations is practically beyond feasibility. In the mixed FEM methods based on the Lagrange multipliers, the Ladyzhenskaya–Babuška–Brezzi (LBB) condition has to be satisfied to ensure the numerical stability. On the other hand, in meshless methods, functions with a high order of continuity are created in a simple and straightforward manner [3].

Early studies on solving fourth-order differential equations by means of meshless methods included the C1 primal formulations for thin beams and plates, cf.[4, 5]. In order to reduce numerical costs and inaccuracies occurring in the C1 formulations, Atluri and Shen [6] used the mixed Meshless Local Petrov-Galerkin (MLPG) method, originally proposed in [7], for proposing a number of new possible mixed methods to be used for solving fourth-order differential equations. Therein, it is demonstrated that the use of high-continuity meshless

approximations requires high computational costs and causes a considerable loss in the accuracy of numerical solutions due to an inaccurate approximation of higher-order derivatives. In the primal meshless methods based on the weak forms of governing equations, additional degradation of computational efficiency in terms of computational time and numerical stability is caused by a problematic numerical integration of weak forms [8]. Later, Moosavi and others [9] used the mixed MLPG approach to derive a meshless counterpart of the mixed Finite Volume Method (FVM) [10] for the bending of thin beams.

Similar to the bending of thin structures, numerical implementations of strain gradient models often result in complicated numerical FEM algorithms [11], such as primal C1 algorithms [12] or mixed formulations [13, 14]. Again, in contrast to FEM, the development of explicit strain gradient C1 models via primal Galerkin meshless methods is straightforward due to a high continuity order of meshless functions [15], but such approaches are also related to reduced accuracy due to the calculation of high-order derivatives of meshless functions [6]. In the mixed meshless approaches, complications may occur due to the improper imposition of boundary conditions [6] and due to solving large unsymmetrical global systems of equations [9]. At present, the focus has been shifted to the development of nodally integrated [16] and smoothed [17] meshless methods that avoid the integration of weak forms of governing equations as much as possible in order to reduce the computation time while obtaining the numerical stability and accuracy of the numerical method. Furthermore, an intense scientific interest is also shown in the development of fast meshless collocation methods that do not use any numerical integration [18, 19].

Herein, the existing mixed MLPG approach [6] is extended in order to better address some of the mentioned problems. In order to evaluate the potential of the developed methods more easily and to present the general idea and the applied methodology more clearly, only simple one-dimensional (1D) linear problems are considered here, without including any nonlinearities. The primary variable and its gradients up to the third order are approximated by the same interpolating Moving Least Square (IMLS) approximation [20, 21]. Governing equations are based on the local weak forms of the principles of conservation of linear and angular momenta as well as on compatibility conditions between the approximated variables. By choosing appropriate test functions, various methods may be derived. In general, the use of the mixed approach relaxes the continuity requirement on trial functions and enables the use of low-order polynomial bases with small supports, thus improving numerical efficiency in terms of computational costs and stability. Special attention is devoted to proper implementation of the boundary conditions (BCs) needed to obtain well-posed systems of equations. The performance of the presented algorithms is shown by a few representative numerical examples.

The paper is organised as follows: Section 2 presents a general form of the considered governing equations and the derivation of local weak forms for the engineering problems described by fourth-order differential equations. The most important details of the discretisation procedures, including the description of the IMLS approximation and the derived mixed meshless methods, are presented in Section 3. Numerical examples demonstrating the accuracy and performance of the proposed methods are presented in Section 4. In Section 5, some concluding remarks are given.

2. Governing equations and local weak forms

In this paper, we consider a general solution procedure using the mixed MLPG method for fourth-order differential equations of the following type:

$$aw^{(4)} + bw'' + cw - q = 0, \quad \text{in} \quad \Omega. \tag{1}$$

In the above expression, w is the primal variable, and the primed symbols denote the derivatives of w, i.e. w', w'', and w''', which stand for the first, the second, and the third derivative of w with respect to the space variable x, respectively. The following BCs must be prescribed on the global boundary Γ surrounding the global domain Ω

$$\begin{aligned} &w = \overline{w} \text{ on } \Gamma_w, \quad w' = \overline{w}' \text{ on } \Gamma'_w, \quad w'' = \overline{w}'' \text{ on } \Gamma''_w, \quad w''' = \overline{w}''' \text{ on } \Gamma'''_w, \\ &\Gamma = \Gamma_w \cup \Gamma'_w \cup \Gamma''_w \cup \Gamma'''_w, \quad \Gamma_w \cap \Gamma'''_w = \varnothing, \ \ \Gamma'_w \cap \Gamma''_w = \varnothing, \end{aligned} \tag{2}$$

where Γ_w, Γ'_w, Γ''_w and Γ'''_w denote the parts of Γ with prescribed values for w, w', w'', and w''', respectively. The physical meaning of the parameters a, b, c, and q depends on the problem considered.

According to the mixed MLPG approach, w, w', w'' and w''' may all be considered as unknown system variables, which can be approximated by separate meshless approximations. In the following text, the substitution $\{w, w', w'', w'''\} = \{u_1, u_2, u_3, u_4\}$, together with $\Gamma_{u1} = \Gamma_w$, $\Gamma_{u2} = \Gamma'_w$, $\Gamma_{u3} = \Gamma''_w$, $\Gamma_{u4} = \Gamma'''_w$, is used. The compatibility conditions between the variables then read as

$$u_2 = u_1', \ \ u_3 = u_2', \ \ u_4 = u_3'. \tag{3}$$

Now, the local weak forms (LWF) of (3) and (1) may be written over a local sub-domain Ω_S positioned inside Ω [3], $\Omega_S \subset \Omega$, as

$$\begin{aligned} &\int_{\Omega_S} v_1 \left(u_1' - u_2 \right) \mathrm{d}\Omega = 0, \quad \int_{\Omega_S} v_2 \left(u_2' - u_3 \right) \mathrm{d}\Omega = 0, \quad \int_{\Omega_S} v_3 \left(u_3' - u_4 \right) \mathrm{d}\Omega = 0, \\ &\int_{\Omega_S} v_4 \left(a u_4' + b u_2' + c u_1 - q \right) \mathrm{d}\Omega = 0. \end{aligned} \tag{4}$$

Herein, v_i, $i = 1,2,3,4,$ are the arbitrarily chosen, kinematically admissible test functions. Depending on the choice of the test functions, various numerical methods may be derived.

3. Numerical implementation

3.1 Discretisation

The global domain Ω is discretised by a set of N nodes $x_I, I = 1,2,...,N$. Around each node I, a local sub-domain, Ω_S^I, is defined, bounded by a local boundary, Γ_S^I, as shown in Figure 1.

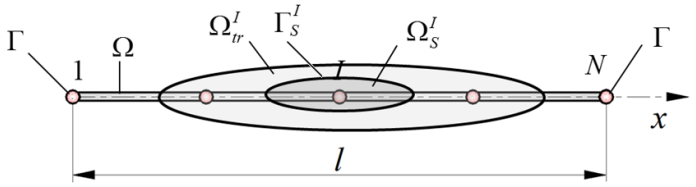

Fig. 1 Discretised model

The weak form (4) is written for each Ω_S^I and all variables u_i are approximated by using the same IMLS approximation, which leads to

$$u_i(x) = \sum_{J=1}^{N} \phi_J(x) \left(\hat{u}_i \right)_J, \quad i = 1,2,3,4 \ . \tag{5}$$

Herein, ϕ_J and $\left(\hat{u}_i\right)_J$ represent the one-dimensional (1D) meshless nodal shape function and the nodal value of the variable u_i for the node *J*, respectively. Since the well-known MLS functions are utilised for a meshless approximation, cf. [3, 22], only main relations are presented here. The MLS nodal shape function $\phi_J\left(x\right)$ is defined as

$$\phi_J\left(x\right)=\mathbf{p}^{\mathrm{T}}\left(x\right)\left[\mathbf{A}^{-1}\left(x\right)\mathbf{B}\left(x\right)\right]_J, \tag{6}$$

where $\mathbf{A}\left(x\right)$ is the momentum matrix defined as

$$\mathbf{A}\left(x\right)=\sum_{J=1}^{N}W_J\left(x\right)\mathbf{p}\left(x_J\right)\mathbf{p}^{\mathrm{T}}\left(x_J\right), \tag{7}$$

and the matrix $\mathbf{B}\left(x\right)$ reads as

$$\mathbf{B}\left(x\right)=\left[W_1(x)\mathbf{p}(x_1)\quad W_2(x)\mathbf{p}(x_2)\quad\cdots\quad W_J\left(x\right)\mathbf{p}\left(x_J\right)\quad\cdots\quad W_N\left(x\right)\mathbf{p}\left(x_N\right)\right]. \tag{8}$$

To improve the conditioning of the matrix **A,** the complete monomial basis **p** is expressed in terms of local normalised coordinates, as presented in [23]. $W_J\left(x\right)$ is the weight function associated with the node x_J. Herein, a regularised weight function, similar to that in [20], is utilised to ensure more accurate enforcement of the Kronecker delta property on the IMLS shape function, i.e. $\phi_J\left(x_I\right)\approx\delta_{JI}$. It is to be noted that the node *I* will influence the values of approximated variables u_i only at the points positioned in the weight function support domain Ω_{tr}^{I}. By inserting the approximations (5) into (4), a system of four linear algebraic equations is derived for each node. A global system of equations is obtained by writing the equations in a node-by-node fashion [3, 22]. Table 1 shows the acronyms of the methods presented in this study, together with the applied test functions; these are given in order to facilitate the reading of further text.

Table 1 Numerical methods and test functions applied in this study

Method	Acronym	Test functions			
		v_1	v_2	v_3	v_4
Modified Mixed Meshless Local Petrov-Galerkin (MLPG) method of the second kind	mm-MLPGv2	Heaviside	Dirac	Dirac	Dirac
Mixed Meshless Finite Volume Method	mMFVM	Heaviside	Heaviside	Heaviside	Heaviside
Mixed MLPG approach based on the momentum principle	mMLPGmp	Heaviside	Heaviside	Dirac	Dirac

3.2 Modified mixed Meshless Local Petrov-Galerkin method of the second kind (mm-MLPGv2)

As proposed in [6], the Heaviside function may be chosen as the test function v_4, while the Dirac functions can be employed as v_1, v_2, and v_3, enforcing the compatibility equations (3) only at the nodes. In [6], such method was named the mixed meshless local Petrov-Galerkin method of the second kind. In our numerical experiments, it has been established that this method may become numerically unstable in some cases and that such problems are caused by the procedures used there to impose the BCs. Therefore, here the BCs for u_2 and u_3 are enforced by a collocation procedure in the weighted least squares sense, similar to [24]. For a node x_I,the system (4) can then be transformed into

$$
\begin{aligned}
&\frac{1}{1+\beta_I^2}u_1'(x_I)-u_2(x_I)=-\frac{\beta_I^2}{1+\beta_I^2}\overline{u}_2(x_I),\\
&\frac{1}{1+\gamma_I^2}u_2'(x_I)-u_3(x_I)=-\frac{\gamma_I^2}{1+\gamma_I^2}\overline{u}_3(x_I),\qquad u_3'(x_I)-u_4(x_I)=0,\\
&\int\limits_{L_S^I\cup\Gamma_{SU3}^I} n b u_2\,\mathrm{d}\Gamma+\int\limits_{L_S^I\cup\Gamma_{SU1}^I} n a u_4\mathrm{d}\Gamma+\int\limits_{\Omega_S^I} c u_1\,\mathrm{d}\Gamma=\\
&=-\int\limits_{\Gamma_{SU4}^I} n a\overline{u}_4\,\mathrm{d}\Gamma-\int\limits_{\Gamma_{SU2}^I} n b\overline{u}_2\,\mathrm{d}\Gamma+\int\limits_{\Omega_S^I} q\,\mathrm{d}\Gamma.
\end{aligned}
\tag{9}
$$

In the above equations, β_I and γ_I are the penalty factors, with $\beta_I >> 1$ if $x_I \in \Gamma_{u2}$ and 0 otherwise, and $\gamma_I >> 1$ if $x_I \in \Gamma_{u3}$ and 0 otherwise. Note that both $\overline{u}_2$ and $\overline{u}_4$ appear as the natural BCs in the last equation. However, for the considered problems, either only one of these variables appear in the LWF (9), or both $\overline{u}_2$ and $\overline{u}_4$ have to be prescribed simultaneously at a point on the outer boundary in order to describe relevant BCs properly. For example, in the bending of thin beams, $b = 0$ and the terms containing u_2 are omitted, while in the thin beam buckling problems, u_2 and u_4 are both associated with the transversal force and are therefore prescribed simultaneously on the parts of Γ with the prescribed transversal forces. If $x_I \in \Gamma_{u1} = \Gamma_w$, then $u_1 = \overline{u}_1$ is enforced at the node I instead of the fourth equation in (9). Now, all BCs are properly imposed.

All variables u_i are approximated by employing the same IMLS function approximation scheme. The compatibility conditions at the nodes are then fulfilled accurately and the coefficient matrix of the global discretised system of equations is sparsely populated. Furthermore, for the interpolating meshless approximation schemes, the size of the global system of equations can be relatively easily reduced by successively computing the nodal values of u_2, u_3 and u_4 from the first three equations in (9) and by inserting them in the fourth equation, in much the same way as in [6].

3.3 Mixed Meshless Finite Volume Method (mMFVM)

The same as in the formulation for thin beams [9], all test functions in (4) are chosen to be the Heaviside functions, which leads to a form of the mixed meshless finite volume method. Then, by performing the integration by parts and by applying the Gauss theorem to all expressions in (4), and after discretisation by the meshless IMLS functions (5), the system of equations for the node I can be written as

$$
\sum_{J=1}^{N}\mathbf{K}_{IJ}\,\hat{\mathbf{U}}_J=\mathbf{R}_I,
\tag{10}
$$

where $\mathbf{K}_{IJ}$ stands for the contribution of the node J to the stiffness of the local subdomain of the node I, Ω_S^I. $\hat{\mathbf{U}}_J$ is the vector that collects the nodal variables at the node J, and $\mathbf{R}_I$ is the nodal force vector at the node I, defined as

$$
\mathbf{R}_I=\left[-\int\limits_{\Gamma_{SU1}^I} n\overline{u}_1\,\mathrm{d}\Gamma\quad -\int\limits_{\Gamma_{SU2}^I} n\overline{u}_2\,\mathrm{d}\Gamma\quad -\int\limits_{\Gamma_{SU3}^I} n\overline{u}_3\,\mathrm{d}\Gamma\quad \int\limits_{\Omega_S^I} q\,\mathrm{d}\Gamma-\int\limits_{\Gamma_{SU4}^I} n a\overline{u}_4\,\mathrm{d}\Gamma-\int\limits_{\Gamma_{SU2}^I} n b\overline{u}_2\,\mathrm{d}\Gamma\right]^{\mathrm{T}}.
\tag{11}
$$

Herein, n denotes the outward unit normal vector to the global boundary. All BCs are defined as natural BCs and are imposed in the weak form. All non-zero terms of the matrix

$\mathbf{K}_{IJ}$ are integrals over Ω_S^I and parts of the local boundary Γ_S^I. Due to the integration, the global stiffness matrix is in general more populated than in the mMLPGv2 method presented in the previous chapter, which increases somewhat the total numerical costs. A reduction in the size of the global discretised equation system by a successive elimination of nodal variables associated with higher-order derivatives is still possible, but it is costlier than in the previous method. The matrix manipulation required for achieving such a reduction includes the matrix inversion, besides the matrix adding and multiplication.

3.4 Mixed MLPG approach based on the momentum principle (mMLPGmp)

Here, the Dirac function is used for the test functions v_1 and v_2, while the Heaviside function is employed as v_3 and v_4, which leads to

$$\begin{gathered}\left(u_1'-u_2\right)\big|_{x=x_I}=0,\quad \left(u_2'-u_3\right)\big|_{x=x_I}=0,\quad \int\limits_{L_S^I\cup\Gamma_{SU2}^I} n\,u_3\,\mathrm{d}\Gamma-\int\limits_{\Omega_S^I} f\,u_4\,\mathrm{d}\Gamma=-\int\limits_{\Gamma_{SU3}^I} n\,\overline{u}_3\,\mathrm{d}\Gamma,\\ \int\limits_{L_S^I\cup\Gamma_{SU3}^I} n\,b\,u_2\,\mathrm{d}\Gamma+\int\limits_{L_S^I\cup\Gamma_{SU1}^I} n\,a\,u_4\,\mathrm{d}\Gamma+\int\limits_{\Omega_S^I} c\,u_1\,\mathrm{d}\Gamma=-\int\limits_{\Gamma_{SU4}^I} n\,a\,\overline{u}_4\,\mathrm{d}\Gamma-\int\limits_{\Gamma_{SU2}^I} n\,b\,\overline{u}_2\,\mathrm{d}\Gamma-\int\limits_{\Omega_S^I} q\,\mathrm{d}\Gamma.\end{gathered}\tag{12}$$

It is to be noted that the first two equations represent the compatibility conditions between u_1, u_2 and u_3, which are in general associated with the kinematic variables of a considered problem (e.g. deflection, slope, and curvature in thin beams) at the nodes. Likewise, it can be shown that the last equation can be interpreted as the weak form of the linear momentum principle for Ω_S^I (e.g. the equilibrium equation of forces in the transversal direction in the beam bending). Finally, the third equation stems from the angular momentum principle for Ω_S^I (e.g. the equilibrium equation of moments in the beam bending). Now, only the prescribed values for u_3 and u_4, i.e. $\overline{u}_3$ and $\overline{u}_4$, appear as the natural BCs in (12), which can be associated with dynamical system variables, such as the bending moments and transversal forces in the beam bending or the tractions in the gradient elasticity. The BCs for u_1 and u_2 are prescribed by setting $u_1=\overline{u}_1$ and $u_2=\overline{u}_2$ at the node I instead of the third and the fourth equation in (12), respectively.

After applying the approximations (5), the nodal values for u_2 and u_3 can be eliminated from the system of equations in a simple and efficient way by a successive calculation and substitution from the first two equations in (12), analogous to the MLPG method of the second kind mm-MLPGv2 presented in chapter 3.2. Consequently, the global discretised system of equations is then reduced to only two equations per node, representing the linear and the angular momentum principle over Ω_S^I.

4. Numerical examples

4.1 Simply supported thin beam

The first representative example is the bending of a simply supported thin beam subjected to the uniformly distributed load q, see Fig. 2. The beam is optionally set on an elastic foundation. For thin beams, the variables $u_i, i=1,2,3,4$ are associated with the deflection, slope, curvature, and the third-order deflection gradient, respectively. The coefficients in equation (1) are then the thin beam flexural stiffness $a=EI$, the foundation stiffness $c=k$, and $b=0$. First, a beam without the elastic foundation, with $EI=5\cdot10^6$, $k=0$, $q=1$ *and* $L=100$, is considered. The interpolating moving least square approximating scheme using the first-order basis, IMLS1, is applied. Discretisations using uniformly distributed nodes along the beam are used.

The convergence results are analysed using relative errors in L2-norms defined as

$$r_{ui} = \frac{\left\| u_i^{num} - u_i^{ex} \right\|_2}{\left\| u_i^{ex} \right\|_2}, \; i = 1,2,3,4, \tag{13}$$

where the superscript *num* is related to the obtained numerical solution, while *ex* refers to the analytical referent solution. The convergence of variables u_1 and u_3, representing deflections and second-order derivatives (curvature), respectively, are shown in Figures 3 and 4.

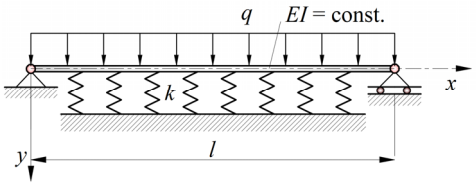

Fig. 2 Simply supported beam subjected to a uniformly distributed load

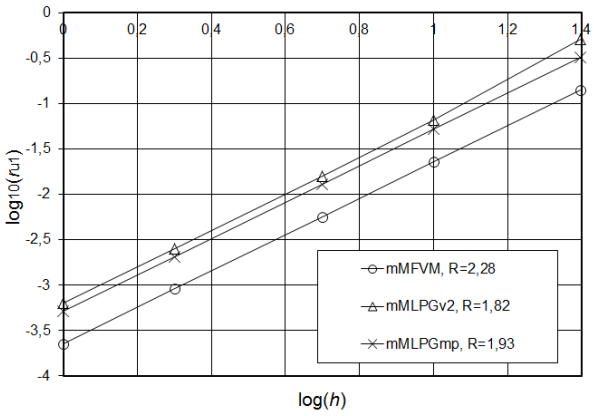

Fig. 3 Convergence of deflections for a simply supported beam

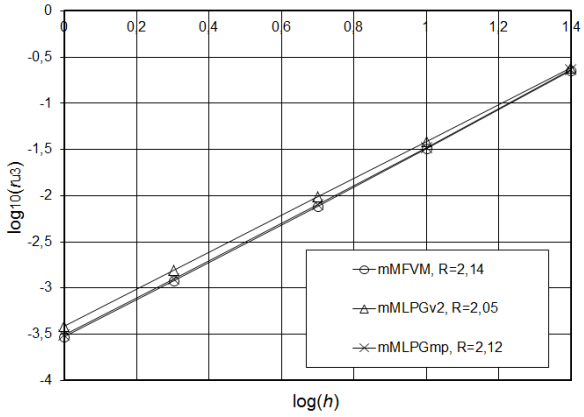

Fig. 4 Convergence of second-order derivatives for a simply supported beam

The convergence rates are given in the figure captions. One can see that the convergence rates and the global accuracy for the second-order derivatives are approximately the same for all methods, but the mixed meshless finite volume method gives somewhat higher accuracy and a higher convergence rate for deflections. However, for both variables, the obtained convergence rates are approximately equal to 2 because of the mixed approach applied, where both variables are approximated separately by the first-order IMLS functions.

A beam on an elastic foundation is considered next, with the following parameters: $EI = 1$, $k = 1$, $q = 1$, and $L = 1$. Numerical results are compared with the analytical solution from [6]. The distributions of deflections and curvature along the beam obtained by using the first-order MLS basis and eleven uniformly distributed nodes along the beam are shown in Figures 5 and 6. Again, the mMFVM method gives more accurate results for deflections while for derivatives, the accuracy of all methods is very similar. A closer inspection of the results in Figs. 5 and 6 reveals certain oscillations in the variable distributions, clearly visible in the deflections obtained by the mixed MLPG of the second kind. Such oscillations are least pronounced in the mMFVM method, which is based only on the weak forms of the governing equations; this results in the better accuracy of this method. It may be concluded that the oscillations are caused by the sub-optimal sampling of the higher-order variables $u_i; i = 2,3,4$ in the methods where the collocation is employed for compatibility equations, i.e. the mm-MLPGv2 and mMLPGmp methods, similar to [25]. It has to be noted that inaccurate numerical integration, inherent to all meshless methods, may

also contribute to such behaviour, cf. [3,8,16]. The results also imply that the issue of numerical stability of the presented methods, typical of all mixed numerical approaches where more than one variable is approximated, has to be investigated in detail.

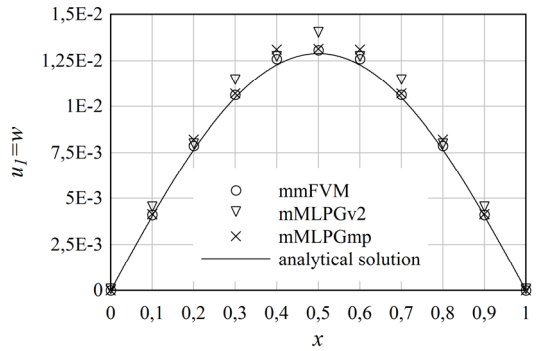

Fig. 5 Deflections for the beam on an elastic foundation

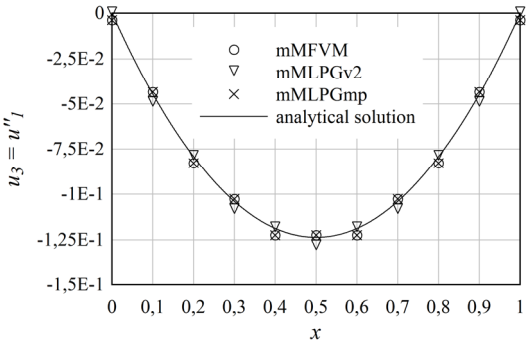

Fig. 6 Second derivatives (curvature) for the beam on an elastic foundation

4.2 Buckling of the elastic beam

The second example deals with the buckling of an elastic beam under the compressive load P, optionally set on an elastic foundation, as shown in Fig. 7.

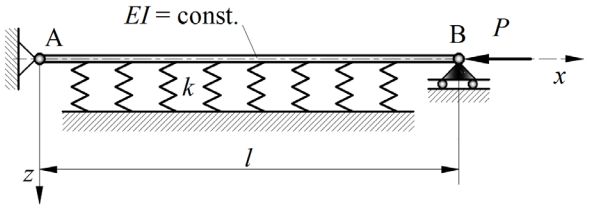

Fig. 7 Beam on an elastic foundation subjected to a buckling load

In this example, the coefficients in (1) are the flexural stiffness $a = EI$, the foundation stiffness $c = k$, and the compressive axial load $b = P$. In numerical calculations only the mixed meshless finite volume method has been applied.

Firstly, buckling without the elastic foundation is considered (k = 0). Herein, the beam with the geometry and material data EI = 1 and l = 1 is chosen. The IMLS approximation functions using the third-order basis, IMLS3, and the discretisations using five nodes are employed. In this problem, the solution procedure consists of finding eigenvalues (buckling loads) and the corresponding eigenvectors (buckling mode shapes). The numerical analysis of the fundamental buckling load is carried out and the compressive load $P^n_{cr1} = 20.21$ is obtained, while the exact solution is equal to $P^e_{cr1} = 20.19$. The solution for the corresponding fundamental buckling mode shape is given in Table 2 and shown in Fig. 8. The distribution of the obtained deflection, shown in Fig. 8, is correspondent to the standard well-known buckling form of a free thin beam under compressive loading.

Table 2 Fundamental buckling mode shape of the beam

Node	x	w	φ
1	0.2	0	0.7274
2	0.4	0.1525	0.3886
3	0.6	0.169	-0.248
4	0.8	0.0675	-0.4524
5	1	0	0

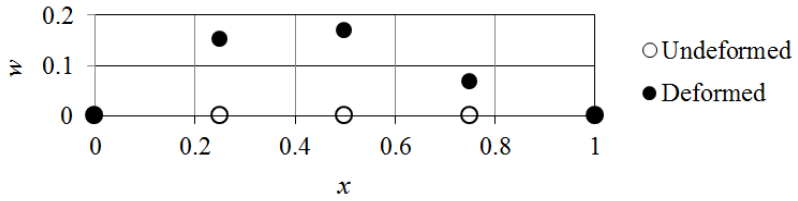

Fig. 8 Deformation of the beam subjected to a buckling load

Next, the buckling of the beam on the elastic foundation is analysed. The beam with the identical geometry and material data as in the previous case is considered; it is set on the foundation with a stiffness of $k = 800$. The obtained solution for the fundamental buckling load in this case was equal to $P_{cr1}^{n} = 59.9$, while the analytical solution is $P_{cr1}^{e} = 60.2$. The corresponding fundamental buckling mode shape shown in Fig. 9 is different from that in the previous case. It can be seen from the presented results that for this eigenvalue problem, the proposed mixed finite volume method yields a less than 1% error for a critical force, which is often acceptable for practical applications, even if coarse discretisation is used.

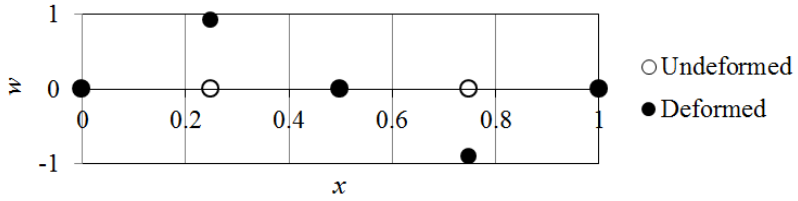

Fig. 9 Deformation of the beam on elastic foundation subjected to a buckling load

4.3 Axial bar in gradient elasticity

A bar in gradient elasticity subjected to the axial load as shown in Fig. 10 is considered as the final example. Here, a nonlocal material model with only one internal parameter [11] is employed; the model is described by the following constitutive equation

$$\sigma = E\,\varepsilon - l^2 E\,\eta = E\,u' - l^2 E u'' \,, \tag{14}$$

where u is the axial displacement, $\varepsilon = u'$ is the strain, and $\eta = u''$ is the second-order displacement gradient, i.e. the strain gradient. As before, the primed values denote the derivatives of u with respect to the space variable x. E is the Young modulus and l is the material parameter related to the material microstructure.

By applying the 1D strain gradient elasticity model (14), the equilibrium equation written in terms of displacements will acquire the form (1), with u instead of w. Therein, the coefficients in LWF (4) are $a = -l^2 E$, $b = E$, and $c = 0$, with the variables $u_i, i = 1,2,3,4$ associated with the displacement, strain, and the second- and third-order displacement gradients, respectively. The bar has a cross-section surface of $A = 4$ and a length of $L = 100$. The Young modulus is $E = 210000$. The left side of the bar is clamped; on the right side, the force $\overline{P} = 4$ is applied, as shown in Fig. 10. The applied boundary conditions in gradient elasticity are taken as $u(0) = 0$, $R(0) = -Al^2 E u''(0) = 0$, $u'(L) = \varepsilon_o = 0.5$ and $P(L) = A(Eu'(L) - l^2 E u'''(L)) = \overline{P}$. Here, P and R stand for the tractions and double-tractions, respectively.

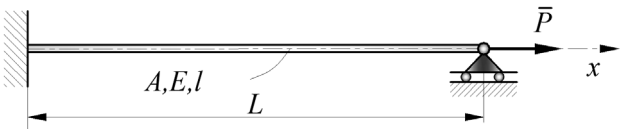

Fig. 10 Axial bar in gradient elasticity

In numerical calculations, only the mixed meshless finite volume method has been applied, and the first-order basis in the MLS scheme is utilised for the approximation of all variables. Numerical models with eleven uniformly distributed discretisation nodes are used in all calculations. The influence of the different values of the microstructural parameter l on the deformation of the bar (size effect) is examined. The obtained displacement, strain, and second-order displacement gradient distributions are shown in Figs. 11 to 13in comparison to the analytical solutions from [25].

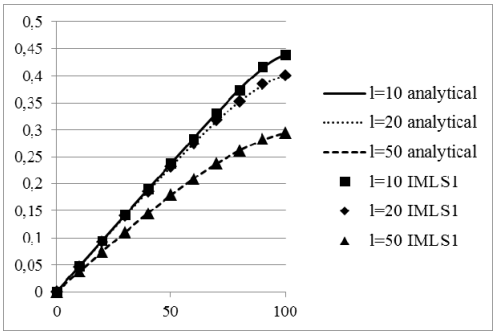

Fig. 11 Displacements on the bar - microstructural parameter l

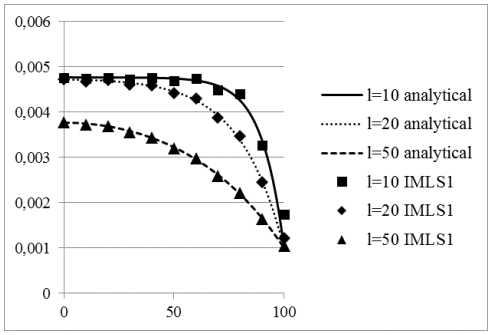

Fig. 12 Strains (first derivatives) on the bar - microstructural parameter l

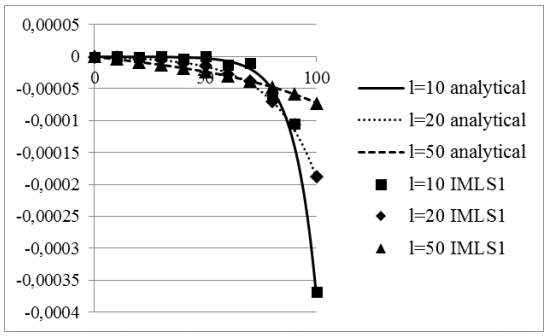

Fig. 13 Second-order displacement gradient on the bar -microstructural parameter l

The obtained results show good agreement with the analytical solutions even with the low-order basis used. Hence, it can be stated that the proposed method exhibits considerable potential for the applications where the gradient elasticity might be needed, such as the modelling of the size effect or stress distributions around a crack tip.

5. Conclusion and further research

The application of the mixed meshless local Petrov-Galerkin approach for solving fourth-order differential equations has been presented. Three different methods have been derived by choosing various test functions. Various methods to be used for a proper implementation of the boundary conditions needed for obtaining well-posed systems of equations are presented and commented. The numerical experiments dealing with the bending of thin beams have shown that all the methods possess almost identical convergence rates for all approximated variables. The mixed meshless finite volume method yields the most accurate response in the primary variable. This method is further successfully adapted to the application in gradient elasticity. In all examples, accurate results have been obtained even with a low order of the meshless approximation functions. The presented results imply that the developed mixed MLPG methods are suitable for modelling the engineering problems described by fourth-order differential equations. Therefore, they will be extended and used for solving two- and three-dimensional problems in the future. Thereby, rigorous tests and

theoretical analyses regarding the numerical and computational efficiency are needed, in line with those performed for the existing mixed MLPG methods, cf. [3,19,21,25], in order to correctly assess the applicability of the proposed methods. In addition, further research is needed to investigate the applicability of the presented methods to solving nonlinear problems. Although a more detailed analysis in that direction is needed, we believe that in this initial phase, the mixed meshless finite volume method is a good candidate for further extension in that direction due to its higher accuracy and seemingly better stability. It is well known that the performance of methods based on the collocation might by overly dependent on the sampling of the points used for the collocation, which in general becomes more pronounced in a nonlinear setting, especially when irregular discretisation patterns are employed.

Acknowledgement The first author would like to acknowledge the Fulbright Scholarship that allowed him to stay at the UCI during his research. This study has also been partly supported by the Croatian Science Foundation under the project Multiscale Numerical Modeling of Material Deformation Responses from Macro- to Nanolevel (2516).

REFERENCES

[1] G. Engel, K. Garikipati, T.J.R. Hughes, M.G. Larson, L. Mazzei, R.L. Taylor, Continuous/discontinuous finite element approximations of fourth-order elliptic problems in structural and continuum mechanics with applications to thin beams and plates, and strain gradient elasticity, Computer Methods in Applied Mechanics and Engineering, 191 (2002) 3669-3750. https://doi.org/10.1016/s0045-7825(02)00286-4

[2] P. Fischer, J. Mergheim, P. Steinmann, On the C1 continuous discretization of non-linear gradient elasticity: A comparison of NEM and FEM based on Bernstein–Bézier patches, International Journal for Numerical Methods in Engineering, 82 (2010) 1282-1307. https://doi.org/10.1002/nme.2802

[3] S.N. Atluri, The Meshless Method (MLPG) for Domain & BIE Discretization, Tech Science Press, Forsyth, USA, 2004.

[4] P. Krysl, T. Belytschko, Analysis of thin plates by the element-free Galerkin method, Computational Mechanics, 17 (1995) 26-35. https://doi.org/10.1007/s004660050089

[5] S.N. Atluri, J.Y. Cho, H.-G. Kim, Analysis of thin beams, using the meshless local Petrov–Galerkin method, with generalized moving least squares interpolations, Computational Mechanics, 24 (1999) 334-347. https://doi.org/10.1007/s004660050456

[6] S.N. Atluri, S. Shen, Simulation of a 4th Order ODE: Illustration of Various Primal & Mixed MLPG Methods, CMES: Computer Modeling in Engineering & Sciences, 7 (2005) 241-268.

[7] S.N. Atluri, Z.D. Han, A.M. Rajendran, A New Implementation of the Meshless Finite Volume Method, Through the MLPG "Mixed" Approach, CMES: Computer Modeling in Engineering & Sciences, 6 (2004) 491-514.

[8] T. Jarak, J. Soric, Analysis of rectangular square plates by the mixed Meshless Local Petrov-Galerkin (MLPG) approach, CMES: Computer Modeling in Engineering & Sciences, 38 (2008) 231-261. https://doi.org/10.1007/978-1-4020-9231-2_19

[9] M.R. Moosavi, F. Delfanian, A. Khelil, The orthogonal meshless finite volume method for solving Euler–Bernoulli beam and thin plate problems, 2011. https://doi.org/10.1016/j.tws.2011.03.001

[10] E. Oñate, M. Cervera, O.C. Zienkiewicz, A finite volume format for structural mechanics, International Journal for Numerical Methods in Engineering, 37 (1994) 181-201. https://doi.org/10.1002/nme.1620370202

[11] H. Askes, E.C. Aifantis, Gradient elasticity in statics and dynamics: An overview of formulations, length scale identification procedures, finite element implementations and new results, International Journal of Solids and Structures, 48 (2011) 1962-1990. https://doi.org/10.1016/j.ijsolstr.2011.03.006

[12] S.A. Papanicolopulos, A. Zervos, I. Vardoulakis, A three-dimensional C1 finite element for gradient elasticity, International Journal for Numerical Methods in Engineering, 77 (2009) 1396-1415. https://doi.org/10.1002/nme.2449

[13] L. Zybell, U. Muehlich, M. Kuna, Z. L. Zhang, A three-dimensional finite element for gradient elasticity based on a mixed-type formulation, 2012. https://doi.org/10.1016/j.commatsci.2011.02.026

[14] E. Amanatidou, N. Aravas, Mixed finite element formulations of strain-gradient elasticity problems, Computer Methods in Applied Mechanics and Engineering, 191 (2002) 1723-1751. https://doi.org/10.1016/s0045-7825(01)00353-x

[15] Z. Tang, S. Shen, S.N. Atluri, Analysis of materials with strain-gradient effects: A Meshless Local Petrov-Galerkin(MLPG) approach, with nodal displacements only, Cmes-Computer Modeling in Engineering & Sciences, 4 (2003) 177-196.

[16] M. Hillman, J.S. Chen, Performance Comparison of Nodally Integrated Galerkin Meshfree Methods and Nodally Collocated Strong Form Meshfree Methods, in: E. Oñate, D. Peric, E. de Souza Neto, M. Chiumenti (Eds.) Advances in Computational Plasticity: A Book in Honour of D. Roger J. Owen, Springer International Publishing, Cham, 2018, pp. 145-164. https://doi.org/10.1007/978-3-319-60885-3_7

[17] Y. Li, G.R. Liu, An element-free smoothed radial point interpolation method (EFS-RPIM) for 2D and 3D solid mechanics problems, Computers & Mathematics with Applications, 77 (2019) 441-465. https://doi.org/10.1016/j.camwa.2018.09.047

[18] D. Wang, J. Wang, J. Wu, Superconvergent gradient smoothing meshfree collocation method, 2018.

[19] B. Jalušić, J. Sorić, T. Jarak, Mixed meshless local Petrov–Galerkin collocation method for modeling of material discontinuity, Computational Mechanics, 59 (2017) 1-19. https://doi.org/10.1007/s00466-016-1327-6

[20] T. Most, C. Bucher, New concepts for moving least squares: An interpolating non-singular weighting function and weighted nodal least squares, Engineering Analysis with Boundary Elements, 32 (2008) 461-470. https://doi.org/10.1016/j.enganabound.2007.10.013

[21] J. Soric, T. Jarak, Mixed meshless formulation for analysis of shell-like structures, Computer Methods in Applied Mechanics and Engineering, 199 (2010) 1153-1164. https://doi.org/10.1016/j.cma.2009.12.007

[22] G.R. Liu, Mesh Free Methods: Moving beyond the Finite Element Method, CRC Press, Boca Raton, USA, 2003.

[23] T. Jarak, J. Soric, J. Hoster, Analysis of shell deformation responses by the meshless local Petrov-Galerkin (MLPG) approach, CMES: Computer Modeling in Engineering & Sciences, 18 (2007) 235-246. https://doi.org/10.1007/978-1-4020-9231-2_19

[24] S.N. Atluri, H.T. Liu, Z.D. Han, Meshless local Petrov-Galerkin (MLPG) mixed collocation method for elasticity problems, Cmes-Computer Modeling in Engineering & Sciences, 14 (2006) 141-152.

[25] Jarak, T., Sorić, J., On Shear Locking in MLPG Solid-Shell Approach, CMES: Computer Modeling in Engineering & Sciences, 81 (2011) 157-193.

[26] S. Papargyri-Beskou, D. Beskos, Static Analysis of Gradient Elastic Bars, Beams, Plates and Shells, 2010.

Submitted: 22.3.2019

Accepted: 02.3.2020

Tomislav Jarak
Boris Jalušić
Jurica Sorić
University of Zagreb
Faculty of Mechanical Engineering and Naval Architecture
Ivana Lučića 5, 10002 Zagreb, Croatia